Cement & Concrete Composites 33 (2011) 749–762

Contents lists available at ScienceDirect

Cement & Concrete Composites

journal homepage: www.elsevier.com/locate/cemconcomp

Using electrical, magnetic and acoustic sensors to detect damage in segmental concrete pipes subjected to permanent ground displacement

Mohammad Pour-Ghaz [a,*], Junhee Kim [b], Srinivasa S. Nadukuru [b], Sean M. O'Connor [b], Radoslaw L. Michalowski [b], Aaron S. Bradshaw [c], Russell A. Green [d], Jerome P. Lynch [b], Amir Poursaee [e], W. Jason Weiss [f]

[a] Purdue University, School of Civil Engineering, 550 Stadium Mall Drive, West Lafayette, IN 47907, United States
[b] University of Michigan, Department of Civil and Environmental Engineering, 2340 G.G. Brown Bldg., Ann Arbor, MI 48109, United States
[c] Civil and Environmental Engineering, University of Rhode Island, Department of Civil and Environmental Engineering, Kingston, RI 02881, United States
[d] Civil and Environmental Engineering, The Charles Edward Via, Jr. Department of Civil and Environmental Engineering, 120B Patton Hall, Virginia Tech Blacksburg, VA 24061, United States
[e] Civil Engineering, Clemson University, Civil Engineering Department, 316 Lowry Hall, Box 340911, Clemson, SC 29634, United States
[f] Director of the Pankow Materials Laboratory, School of Civil Engineering, Purdue University, School of Civil Engineering, 550 Stadium Mall Drive, West Lafayette, IN 47907, United States

ARTICLE INFO

Article history:
Received 12 November 2010
Received in revised form 7 April 2011
Accepted 8 April 2011
Available online 16 April 2011

Keywords:
Acoustic emission
Conductive concrete
Crack detection
Damage sensing
Earthquake engineering
Electrical sensing
Large-scale test
Magnetic sensing
Permanent ground deformation
Segmental concrete pipeline

ABSTRACT

This paper describes results of an experimental study that used sensing methods for monitoring damage along segmental concrete pipelines resulting from permanent ground displacement across a simulated earthquake fault. The literature contains examples of such damage occurring during actual earthquakes, significantly impacting the functionality of the pipelines. Detecting the location of the damage and the extent of the damage in pipelines can significantly accelerate post-earthquake repair efforts. In this paper, electrical sensing methods, magnetic sensing, and acoustic emission are used to monitor structural damage in a segmental concrete pipeline during a large-scale test. In this test, the segmental concrete pipeline was subjected to a concentrated transverse permanent ground displacements (PGDs). The majority of the damage to the pipe segments was localized at the joints, especially the bell sections while the damage to the spigots was minimal. The damage extended away from the joints in the pipe segments in the immediate vicinity of the fault line. Telescoping (i.e., crushing of the bell-and-spigot) was a primary mode of failure that was observed. The results of this study indicate that electrical sensing methods (including the use of conductive grout), magnetic sensing, and acoustic emission, employed alone or in combination, can detect and quantify the damage in segmental concrete pipelines.

1. Introduction

This paper describes results of an experimental study that used in situ sensing methods to identify damage along segmental concrete pipelines resulting from permanent ground displacement across a ground fault. The literature is replete with examples of such damage occurring during actual earthquakes, adversely impacting the functionality of the pipelines. For example, a report issued 3 days after the 2010 Chile earthquake indicated that more than 1.5 million people were still without access to clean drinking water as a result of the earthquake [1]. Rapid restoration of societal lifelines (such as pipelines) is an absolutely essential component of successful response and recovery efforts [2]. Previous earthquakes, such as the 1994 Northridge earthquake, have shown that the actual repair cost of the pipelines reflects only a fraction of the total costs associated with the failure of lifelines. Indirect losses, such as business losses during downtime and fire damage, which could have been minimized had it not been for the loss of the water supply, can be several times higher than the direct losses [3–5]. Methods for accurate damage detection can significantly accelerate the repair efforts of pipelines and, in turn, minimize the downtime. After the 1995 Kobe earthquake (Kobe, Japan), complete restoration of water and gas pipelines took over 2 and 3 months, respectively, while the electricity was restored in 3 days [6–8]. A major cause of this delayed recovery time was that many water and gas pipelines are buried and not readily accessible for visual inspection.

The seismic hazards that are important for pipelines can be categorized as wave propagation and permanent ground displacement (PGD) [6,9]. Irrespective of the direction in which PGD

* Corresponding author. Tel.: +1 765 494 7999.
E-mail address: pourghaz@purdue.edu (M. Pour-Ghaz).

0958-9465/$ - see front matter © 2011 Elsevier Ltd. All rights reserved.
doi:10.1016/j.cemconcomp.2011.04.004

affects the pipeline (transverse or longitudinal), it can be categorized as concentrated [10] or distributed [6,11–13]. As their names imply, "concentrated" PGD occurs over a relatively short length of the pipeline while "distributed" PGD occurs over a longer length. The most common types of failures observed in segmental concrete pipelines subjected to concentrated transverse PGD can be categorized in four groups: (1) localized damage in the vicinity of the joints: cracking and spalling of the bell-and-spigot connection [2,14,15]; (2) telescoping and crushing of the bell-and-spigot [2,14,16–18]; (3) decoupling due to tensile forces, bending and rotation at joints [19–21]; and (4) extensive cracking of the pipe away from the joints after large PGD [2,15]. Although the common modes of failure of the segmental concrete pipelines are rather well-documented, information on the progression of damage in the vicinity of the concentrated transverse PGD is scarce. Furthermore, effective methods for identifying the location of the damage and the extent of the damage in the segmental concrete pipelines are currently not well developed. For example, the major challenge in detecting damage in buried concrete pipelines is that visual inspection is not feasible, often requiring excavation, which is expensive and time-consuming.

The main objectives of the study presented herein are twofold: (1) to utilize methods for damage detection and health monitoring for segmental concrete pipelines and (2) provide a better understanding of the damage evolution in segmental concrete pipelines in the vicinity of the concentrated transverse PGD using new methods of damage detection. In this vein, six methods were used in this study to monitor deformation and damage of the pipeline during the test; four of those methods, specifically designed for segmental concrete pipelines, are discussed in this paper. The methods that are discussed in the present work include: conductive surface tape sensors (CST), magnetic sensors, acoustic emission (AE), and conductive grout. These methods were implemented on commercial concrete pipe segments that were used in a large-scale test under simulated PGD. The methods were designed to not only detect the most common modes of failure, but more importantly to detect damage in its initial stages. The two methods used in the test that are not discussed in great detail in this paper are strain gages and LVDTs. In the subsequent sections of this paper, an overview of the large-scale test facility (George E. Brown, Jr. Network for Earthquake Engineering Simulation (NEES) site at Cornell University) used in this study is first presented. Next, a description of the concrete pipe tested is given including the method used to place the pipe and to bury it with consolidated backfill. This is followed by a description of the instrumentation, test procedures and a discussion of the results.

2. Large scale testing facility

Full-scale testing of the segmental concrete pipeline was performed at the Network for Earthquake Engineering Simulations (NEES) Large-Scale Lifelines Testing Facility at Cornell University [22,23]. The segmental concrete pipeline was tested in a split-box test basin; Fig. 1a shows the test basin with buried pipeline ready for testing, with the fault denoted by the dashed line (the fault line is inclined at 50° to the longitudinal axis of the test basin). Fig. 1b shows the test basin with excavated pipeline after the test. The test basin was 3.4 m (≈11 ft) wide and 13.5 m (≈44 1/3 ft) long and 2.3 m (≈7 1/2 ft) deep. The soil-filled portion of the test basin near the fault line was wider than the sections further away from the fault (Fig. 1a); this was to reduce the amount of sand needed for backfilling, without affecting the influence of the box boundaries on the deforming pipeline near the primary fault plane. The pipeline was buried using approximately 100 tons of sand. The moveable (North) portion of the test basin was moved along the fault line, relative to the fixed portion (South). The length of the fixed portion of the test basin was 6.5 m (≈21 1/3 ft). The displacement was induced by four hydraulic actuators and simulates transverse PGD [22,23].

3. Concrete pipe segment and pipeline

Commercial class ¾ reinforced concrete culvert pipes with an inner diameter of 12 in. (34.5 cm), manufactured according to ASTM C 76 [24] and ASTM C 655 [25], were used. The concrete pipe segments were 2.44-m (8.0-ft) long with a wall thickness of 5.1 cm

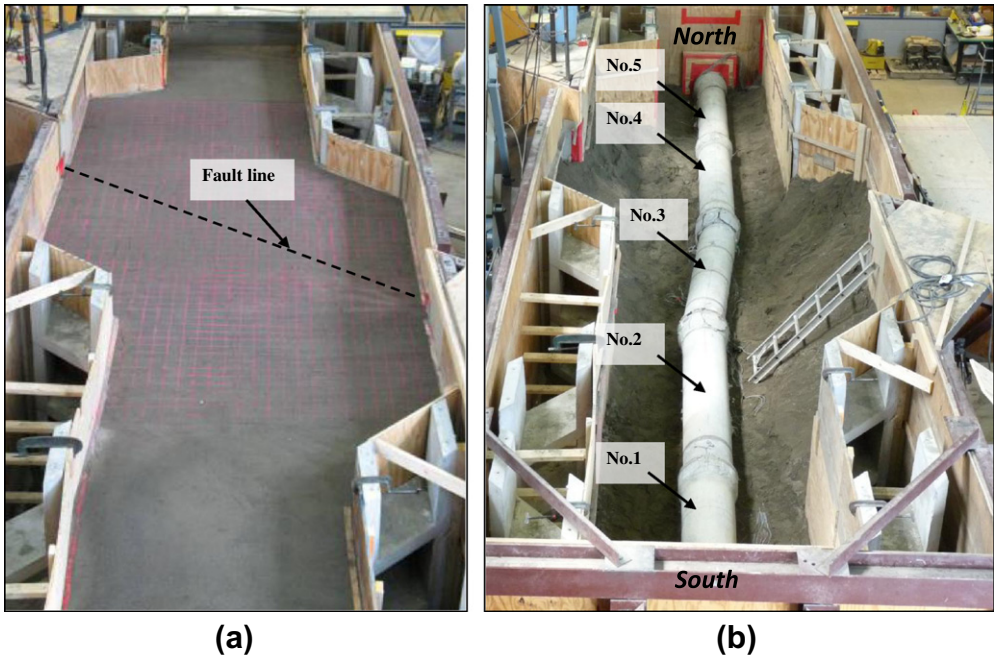

Fig. 1. (a) Test basin after backfilling, (b) full-scale segmental concrete pipeline (after excavation) tested at the large-scale testing facility at the George E. Brown, Jr. Network for Earthquake Engineering Simulation (NEES) site at Cornell University.

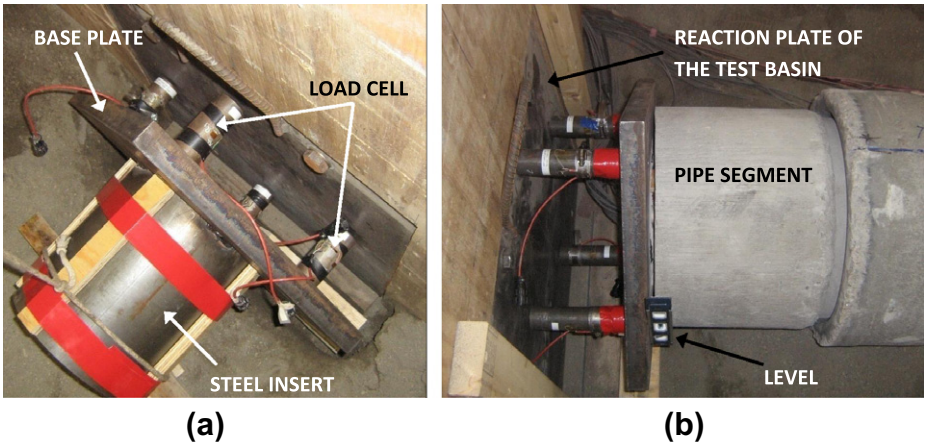

Fig. 2. (a) Heavy steel fixture designed for load transfer from pipe to load cells, (b) north (moveable) end of the pipeline after mounting the fixture.

(≈2 in.). The pipe segments had a circumferential reinforcement ratio of 1.5 cm^2/linear meter length (0.07 $in.^2$/linear ft), and the compressive strength of the concrete was 27.6 MPa (≈4000 psi).

The pipe segments were placed on the prepared bedding (described in the next section) and were aligned using a level and a string spread between the ends of the test basin. A total of five full pipe segments were used; in addition, a 1-foot (30-cm) portion cut from a complete pipe segment was used at the North end to make up the total length of the test basin. The pipe segments were numbered starting from the South end of the test basin (Fig. 1b). The fault line crossed the mid-span of Pipe Segment 3.

All the joints were grouted according to the AWWA C300 [26] standard. A mortar grout with water-to-cement ratio of 0.50 and 30% fine aggregate by volume, conforming to specification of the AWWA C 300 standard [26] was used. To enhance the workability of the grout, 0.5% (by weight of cement) high range water reducer was used. A plastic diaper was placed around the joints to ensure the grout remained in place prior to curing.

Steel plates with inserts were designed for mounting load cells at both ends of the pipeline to monitor the reactions at the end walls of the test basin. The inserts consisted of 1-foot (30-cm) steel hollow tubes (Fig. 2a) mounted on the base plates. The tubes were inserted into the pipe segments at each end of the pipeline, and load cells (4 at each end) were placed between the base plates and the reaction plates on the walls of the test basin (Fig. 2b).

At the South end of the pipeline, the insert was placed inside the spigot of Pipe Segment 1. On the North end, the insert was placed inside the small section of a cut pipe adjacent to the Pipe Segment 5 (Fig. 2b). To avoid contact of the soil and the effect of moisture on the load cells, a wooden box was constructed around the load cells before backfilling the basin with soil.

4. Bedding and backfilling specifications

A 20.0-cm (≈8-in.) thick bedding was prepared by compacting sand using a vibratory plate compactor (plate-tamper). After placing and aligning the pipe segments on the bedding, backfill was placed in 20.0-cm (≈8-in.) lifts. The total height of the backfilling was 140.0 cm (≈55 1/8 in.). Each lift was compacted with the plate-tamper, and the dry unit weight and moisture content were measured using a nuclear density gage according to ASTM D2922 [27] and ASTM D 2216 [28], respectively. Measurements were performed on a grid of 30.0 × 30.0 cm (≈12 × 12 in.) on each compacted lift. The dry unit weight and moisture content of the soil in all layers was 16.5 ± 0.3 kN/m^3 (≈105.8 ± 1.8 lb/ft^3) and 4.2 ± 0.6%, respectively. A grid of 10.0 × 10.0 cm (≈4 × 4 in.) was spray-painted on the surface of the soil after the final lift to aid the visual trace of the deformation of the soil surface (Fig. 1a). This procedure to preparing the pipeline bedding and backfill was intended to closely simulate real field conditions.

5. Instrumentation

The four types of sensors used in the large-scale test to assess damage (i.e., conductive surface tape (CST), magnetic sensors, acoustic emission, and conductive grout) are described below.

5.1. Conductive surface tape

Conductive surface tape (CST) sensors are resistance-based sensors that are installed on the surface of the concrete pipe. The sensors used in this study were made of conductive copper tape. As cracking occurred in the concrete pipe, the CST sensors stretched causing their resistances to rise slightly. When cracks enlarged in the pipe segments, the tape ruptured causing the resistance to increase dramatically. By continuously monitoring the resistance of the conductive surface sensor, the time of cracking can be captured [29]. These sensors were previously used to investigate the effect of boundary conditions and degree of restraint on cracking behavior of the restrained concrete elements [29–31]. These sensors were selected for this work since they are made of a low cost material and can easily and rapidly be applied to the surface of the concrete pipe.

In segmental concrete pipelines subjected to a concentrated transverse PGD, the majority of the damage localizes in the vicinity of the joints [6,16,19]. Therefore, a higher number of CST sensors were installed in the vicinity of the joints. Fig. 3a schematically illustrates an instrumented pipe segment. Photographs of an instrumented bell and an instrumented spigot section of a concrete pipe segment are shown in Fig. 3b.

A total of 24 CST sensors were used to instrument the entire pipeline. Different numbers of CST sensors were used for each pipe segment depending on their relative location with respect to the fault line. Eight CST sensors were installed on Pipe Segment 3 (located on the fault line). The quantity and location of CST sensors shown in Fig. 3a corresponds to that of Pipe Segment 3. Fig. 4 schematically illustrates the complete instrumentation of the pipeline. CST sensors are indicated by the letter "R" (for resistance-based). As may be observed from this figure, six CST sensors were installed on Pipe Segments 2 and 4, and only two CST sensors were installed on each Pipe Segments 1 and 5. In addition to Fig. 4, the detailed location of the CST sensors is also provided in Table 1.

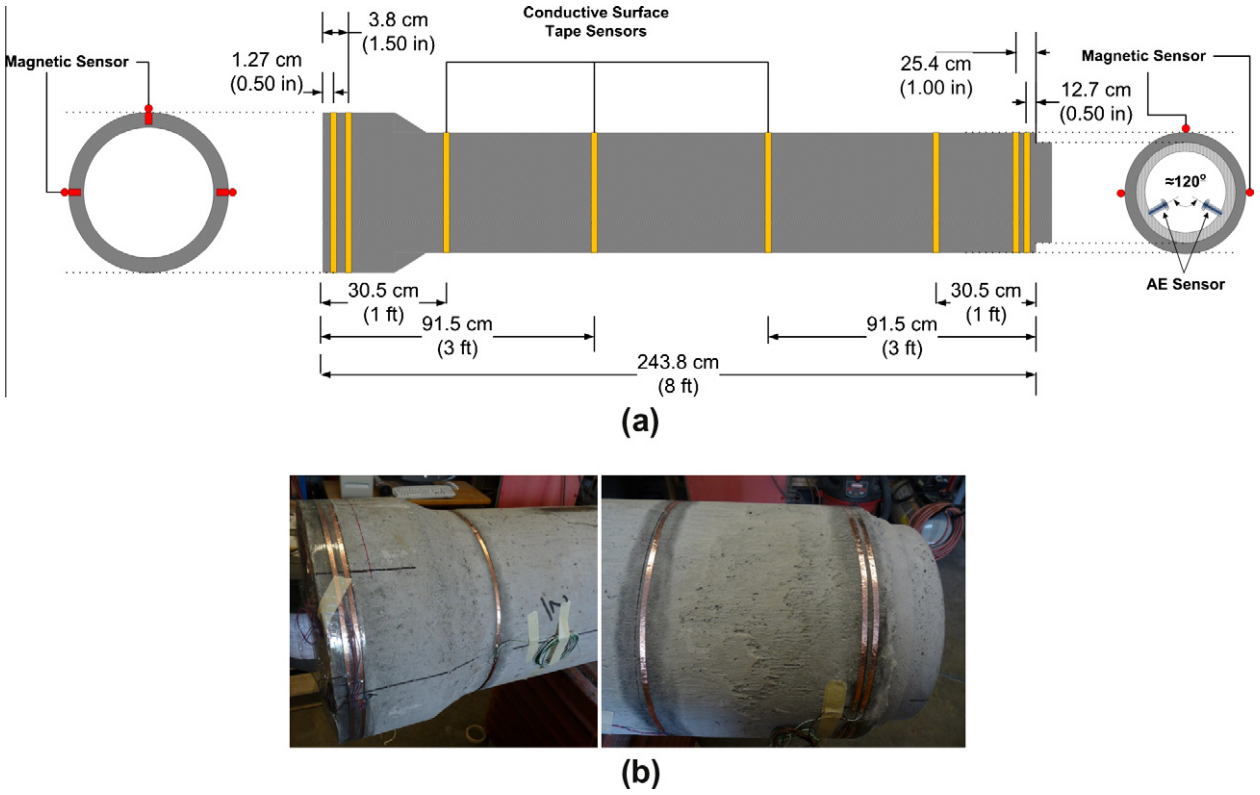

Fig. 3. (a) Schematic illustration of instrumentation on a concrete pipe segment, (b) conductive surface tape sensors installed on the bell and on the spigot section of a concrete pipe segment.

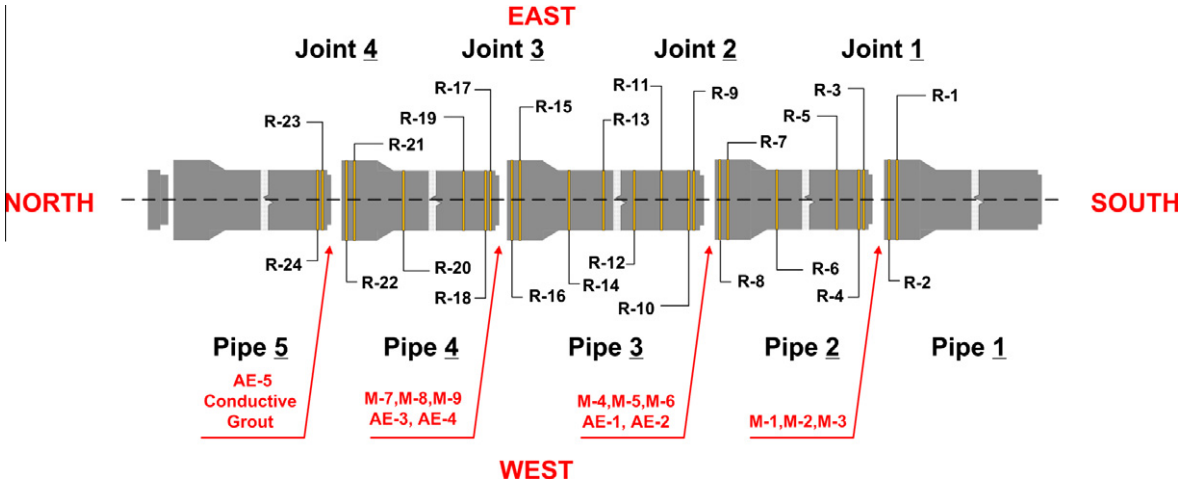

Fig. 4. Schematic illustration of instrumentation of the pipeline and the location of the sensors.

A 24 gage low-resistance copper wire was soldered to the surface of the CST sensors after installation of the sensor on the pipe segments to connect the sensor to an automated resistance measurement unit (AEMS) [32].

5.2. Magnetic opening sensors

Magnetic sensors are two-part sensors consisting of a switch and a magnet. The switch is triggered depending on the strength of the magnetic field, which is dependent on the proximity of the switch and the magnet. In this work, a commercially available standard AC-rated cylindrical mini-magnetic switch was used. The electrical resistance of the switch part of the sensor increases when the distance between the two parts increases more than 2.5 mm (1/10 in.). The responses of the magnetic sensors are monitored by measuring the electrical resistance of the switch. Fig. 5a illustrates both parts of a magnetic sensor used in the present work. These sensors were used to monitor the rotation and separation of the bell and the spigot at each joint. The magnet side of the sensor was installed on the spigot, and the switch side of the sensor was installed on the bell. The two parts of the sensor were installed at a right angle with respect to each other to facilitate triggering of the sensors in response to both decoupling (i.e., opening) and telescoping (i.e., closing) of the joint.

Three magnetic sensors were installed at each joint except the last joint (i.e., Joint 4) at the North end of the pipeline where

Table 1
Type and location of sensors with respect to pipe segments and joints.

Sensor number	Pipe/location	Joint/location
R[a]-1	Pipe 1/Bell	1
R-2	Pipe 1/Bell	1
R-3	Pipe 2/Spigot	1
R-4	Pipe 2/Spigot	1
R-5	Pipe 2/1/8 Spigot side	–
R-6	Pipe 2/1/8 Bell side	–
R-7	Pipe 2/Bell	2
R-8	Pipe 2/Bell	2
R-9	Pipe 3/Spigot	2
R-10	Pipe 3/Spigot	2
R-11	Pipe 3/1/8 Spigot side	–
R-12	Pipe 3/3/8 Spigot side	–
R-13	Pipe 3/3/8 Bell side	–
R-14	Pipe 3/1/8 Bell side	–
R-15	Pipe 3/Bell	3
R-16	Pipe 3/Bell	3
R-17	Pipe 4/Spigot	3
R-18	Pipe 4/Spigot	3
R-19	Pipe 4/1/8 Spigot side	–
R-20	Pipe 4/1/8 Bell side	–
R-21	Pipe 4/Bell	4
R-22	Pipe 4/Bell	4
R-23	Pipe 5/Spigot	4
R-24	Pipe 5/Spigot	4
M[b]-1	–	1/East
M-2	–	1/Top
M-3	–	1/West
M-4	–	2/East
M-5	–	2/Top
M-6	–	2/West
M-7	–	3/East
M-8	–	3/Top
M-9	–	3/West
G[c]-1	–	4/East
G-2	–	4/Top
G-3	–	4/West

[a] CST type sensor.
[b] Magnetic type sensor.
[c] Conductive grout electrode.

conductive grout was used. One sensor was installed at the crown and two sensors were installed at spring lines (Fig. 3a). Both parts of the magnetic sensors were mounted on the pipes using high strength epoxy. The locations of the magnetic sensors along the length of the pipeline are illustrated in Fig. 4, and also are provided in Table 1. Letter M (for magnetic) is used to designate magnetic sensors in Fig. 4 and Table 1.

5.3. Acoustic emission

Cracking of the concrete pipe results in the release of strain energy. The released strain energy leads to stress wave propagation in the pipe. The stress waves cover a wide range of inaudible and audible frequencies, known as acoustic waves. Acoustic emission (AE) describes a technique that captures and monitors the digitized acoustic waves at the surface of the material [33]. Piezoelectric sensors are used to convert the captured acoustic waves into electrical signals. The strength of the signals generally depends on the amount of released energy, distance and orientation of the source with respect to the sensor, and nature of transferring media [30,34–40]. The signal captured with the sensors are then amplified and recorded in a data acquisition system. The calculated energy of the captured acoustic wave is proportional to the fracture energy [35].

AE is particularly powerful since, unlike the previously described methods that require substantial cracking or displacement before damage can be detected, AE can detect damage in the form of micro-cracking that may occur even at very low load levels. These micro-cracks can be detected by acoustic emission before a localized visible crack develops [41].

Two AE sensors were installed at both Joints 2 and 3, which are the closest joints to the fault line (Joints 2 and 3 in Fig. 4), and one AE sensor was installed at Joint 4. All of the AE sensors were installed on the spigot section of the pipe as shown in Fig. 3a. A steel waveguide was used between each sensor and the concrete pipe. Steel waveguides show negligible attenuation [33,42]. The AE sensors were installed on the steel waveguide using silicon-based adhesive as a coupling agent (Fig. 5b). This type of coupling agent has shown good performance in the past for AE sensing. A rigid connection between the waveguide and the concrete was obtained by mounting the waveguide in a small hole drilled in the concrete pipe. A high strength epoxy was used to fix the steel waveguide in place. The complete assembly is shown in Fig. 5b. A pre-amplifier was installed between each sensor and the data acquisition system. The pre-amplifiers were installed inside the pipe segment as shown in Fig. 5c.

5.4. Conductive grout

The conductive grout that was used in this study to monitor the integrity of the joints was a mortar mixture containing highly conductive carbon micro-fibers. The micro-fibers were approximately 7–9 μm (2.75×10^{-4} to 3.5×10^{-4} in.) long and had an aspect ratio (i.e., length/diameter) of approximately 25. The fibers were made of 99% carbon. The conductive grout used was a mortar with a water-to-cement ratio (w/c) of 0.50 and 30% aggregate and 13% carbon micro-fiber by volume.

The volume percentage of the fiber was calculated to be above the theoretical percolation volume. The theoretical percolation volume was calculated based on the theory of overlapping ellipsoids [43]. Trial mixtures with fiber volume above the calculated

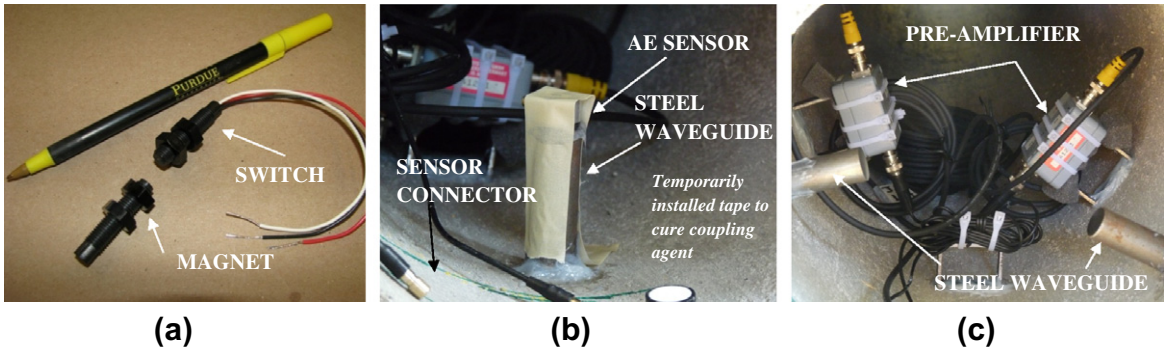

Fig. 5. (a) Components of the magnetic sensor, (b) AE sensors installed on top of a waveguide, (c) waveguide and pre-amplifiers installed inside the pipe segment.

percolation volume were made to optimize the required amount of water reducer (to ensure that the mixture is workable). The grout used had a resistivity value of 0.39 Ω m (≈15.51 Ω in.) after 7 days (in sealed condition). The resistivity of mortar with equivalent non-conductive inclusions was 17.67 Ω m (≈695.61 Ω in.) at the same age.

The electrical resistance of the conductive grout increases with cracking of the grout at the joints (e.g., due to the telescoping failure). By monitoring the electrical resistance of the conductive grout, the damage development at the joint can be assessed. The electrical resistance was measured using three electrodes mounted at 120° with respect to each other around the joint. The electrical resistance was measured between two consecutive electrodes resulting in a total of three sections being measured at each joint. Conductive grout is particularly useful in monitoring the damage due to telescoping failure. Conductive grout was used at the last joint at the north end of the pipeline (Joint 4, see Fig. 4). The locations of the electrodes in the conductive grout are specified in Table 1 and are designated by letter G (for grout).

6. Test procedure

A displacement-controlled testing procedure was used in this experiment. The moveable portion (North end) of the test basin was displaced relative to the fixed portion (South end) in twelve, 2.54-cm (1-in.) steps. In total the North end of the basin was displaced 30.5 cm (12 in.) along the fault in a right lateral strike-slip movement. The magnitude of this displacement was chosen based on the previous test results [2,14,15] and subjected the pipeline to compressive, shear, and bending forces [2,14,15,22,23]. The relative speed of the two portions of the test basins was 0.3 m per minute (≈1 ft per minute). Each displacement step was completed in less than 5 s, after which the test was paused (relaxation phase). The relaxation phase allowed visual inspection of the soil surface, documentation of observations, and examination of the effect of soil relaxation on the axial forces measured by load cells at the both ends of the pipeline.

A high-speed camera was installed above the test basin (approximately 2 m from the soil surface) to capture the soil surface deformation during the experiment. All monitoring systems were activated, and the readings were continuously recorded during the process of displacement.

After the completion of the test and all of the sensor data was collected, the excavation phase began. The first 120 cm (≈47 in.) of the soil was removed using a hydraulic clamshell bucket. The remaining backfill was removed carefully using shovels and brushes to avoid causing further damage to the pipeline. The pipeline after excavation is shown in Fig. 1b.

7. Results and discussion

7.1. Load and displacement

Fig. 6a illustrates the actuator displacement, actuator load, and the total axial load at the North end (moveable end) and the South end (fixed end) of the test basin. The change of load with time at both ends of the test basin shows the same pattern as that of the actuator load. The load at the south end (fixed end) of the test basin slightly lags behind the applied actuator load, especially for the fifth and seventh displacement steps.

The average load in the actuators during the relaxation periods and the average axial forces measured by load cells at both ends of the test basin are plotted in Fig. 6b. This figure is useful for tracing the damage accumulation is the pipeline. The development of damage is accompanied with a dramatic reduction in load due to the increase of the compliance (loss of stiffness) of the system. During the first four applied displacement steps the load in the actuators and at both ends of the pipeline increased with the displacement. During the fifth step, the load slightly decreased in the actuator and a slight increase in the end load was observed at both ends of the pipeline. A significant decrease in load is observed at the seventh displacement step indicating significant damage to the pipeline. Further decrease in load is observed in the twelfth step. It is noted that damage starts to accumulate in the pipeline from the first displacement step; however, it cannot be seen by only looking at the load–displacement plot as the damage up to the seventh step is not significant to increase the compliance of the system to affect the measured loads.

7.2. Conductive surface tape sensors

Before rupture, the CST sensor's resistance is approximately 0.05 Ω. However, after rupture, the resistance increases several orders of magnitude. The resistance measurements are treated as binary, with zero indicating an intact CST (i.e., no damage) and one indicating a ruptured CST (i.e., damaged).

The rupture sequence of the CST sensors is shown in Fig. 7, along with the actuator displacement. Additionally, Fig. 8 shows the location and rupture sequence of the CST sensors on schematics of the pipe segments for six different fault displacements. The arrows in Figs. 7 and 8 indicate the rupture of a CST sensor.

As may be observed from Figs. 7 and 8, significant damage occurred during the second displacement step in the bell sections of Pipe Segments 2 and 3 (Joints 2 and 3, respectively). This damage extended beyond 3.8 cm (≈1½ in.) on the bell section of both pipe segments since both sensors installed on the bell sections of Pipe Segments 2 and 3 detected the damage. The mode of damage that occurred is schematically illustrated in Fig. 9a and can be attributed to the relative rotation of the spigot inside the bell section.

The CST sensor (R-23) installed at the spigot of the Pipe Segment 5 (Joint 4) also detected damage. This sensor was installed 1.27 cm (≈1/2 in.) away from the end of the spigot (see Figs. 3 and 4). The damage, however, is not extensive since the next CST sensor in the array (R-24), which was placed 2.5 cm (≈1 in.) from the end of the spigot (1.27 cm from R-23), did not detect any damage. The damage captured at Joint 4 by R-23 is most likely due to movement of the spigot inside the bell (i.e., "wedge-breaking"). This type of damage is schematically illustrated in Fig. 9b. It is noted that at this stage telescoping of the pipeline is not significant and that the compressive forces along the pipeline only tightened the joints resulting in minimal damage.

With an increase in the displacement during the fourth step (Figs. 7 and 8), further damage developed at Joint 3 where R-17 is located (Fig. 8b). This damage is probably due to wedge-breaking action and did not extend beyond 1.27 cm (≈1/2 in.). Up to the fifth step, the majority of the damage is localized at the joints in the vicinity of the fault line (i.e., Joints 2 and 3). Damage at this point began to occur at Joint 1. The signals slightly lag the displacement of the actuators.

During the fifth and seventh displacement steps, Joints 1 and 4 were damaged and are most likely associated with telescoping effects resulting from high compressive forces. The damage occurred at the bell section of the joints (Figs. 8c and d). Fig. 9c schematically illustrates the damage due to compressive forces (i.e., telescoping).

During the tenth and eleventh displacement steps, damage started to extend beyond the joints and occurred in the body of Pipe Segments 2 and 3 (i.e., R-6 and R-14). These sensors were located 30 cm (≈1 ft) away from the end of the bell section. This type of damage is due to rotation of the pipes at the joints accompanied with compressive axial forces. A schematic illustration of this type of damage is shown in Fig. 9d.

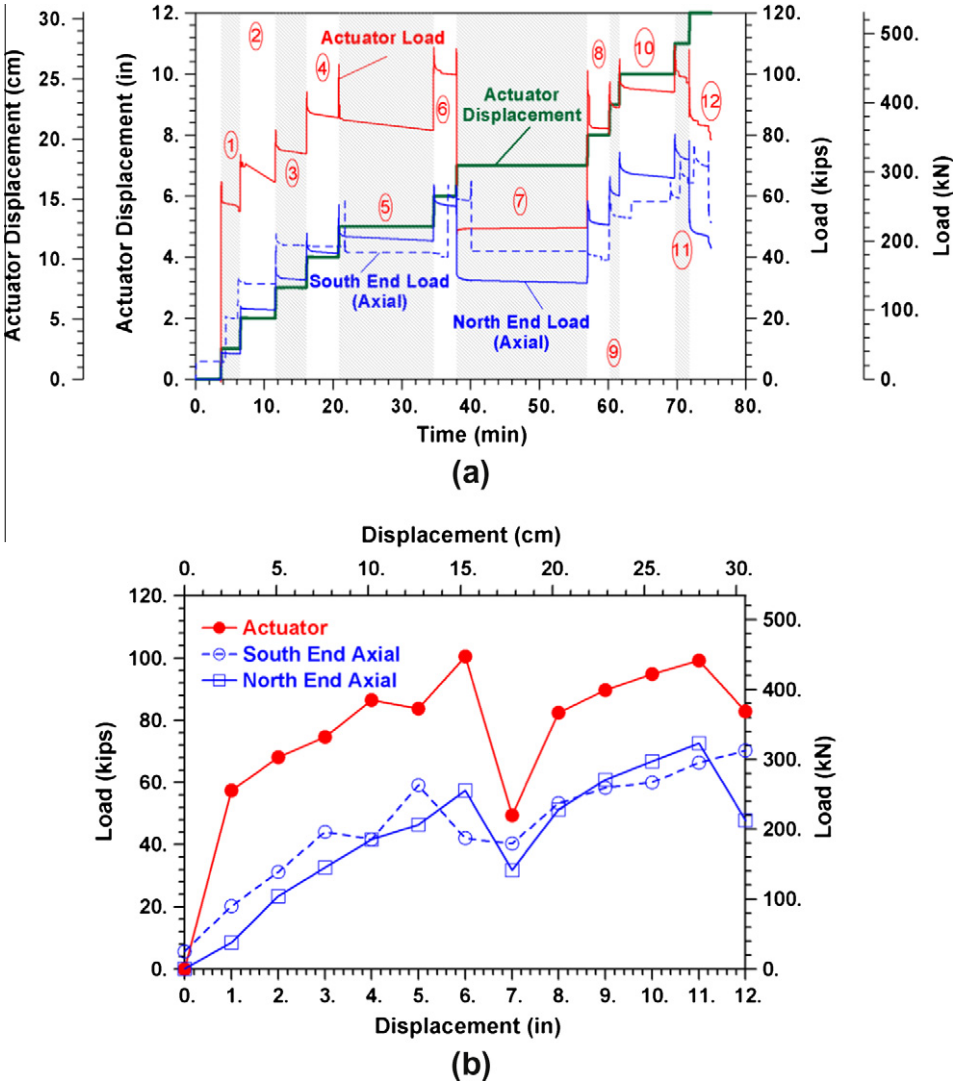

Fig. 6. Actuator displacement, load and the total load at the north (moveable) and south (fixed) end of the test basin.

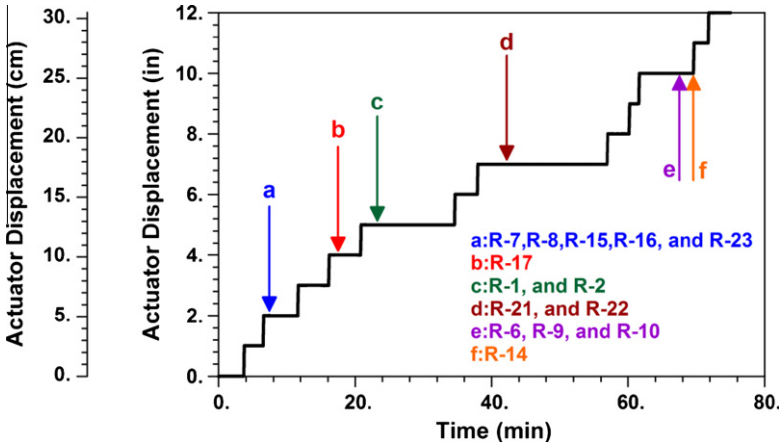

Fig. 7. Sequence of signals received from conductive surface tape (CST) sensors in relation to the actuator displacement.

7.3. Magnetic opening sensors

Fig. 10 shows that the magnetic sensors at Joints 2 and 3 indicate relative movement of the spigot with respect to the bell. These signals are consistent with the signals from CST sensors (Figs. 8a and 11a). A magnetic sensor at the Joint 1 (M-2) also indicates relative displacement of the bell-and-spigot after the third displacement step. There is a slight delay in the response of this sensor,

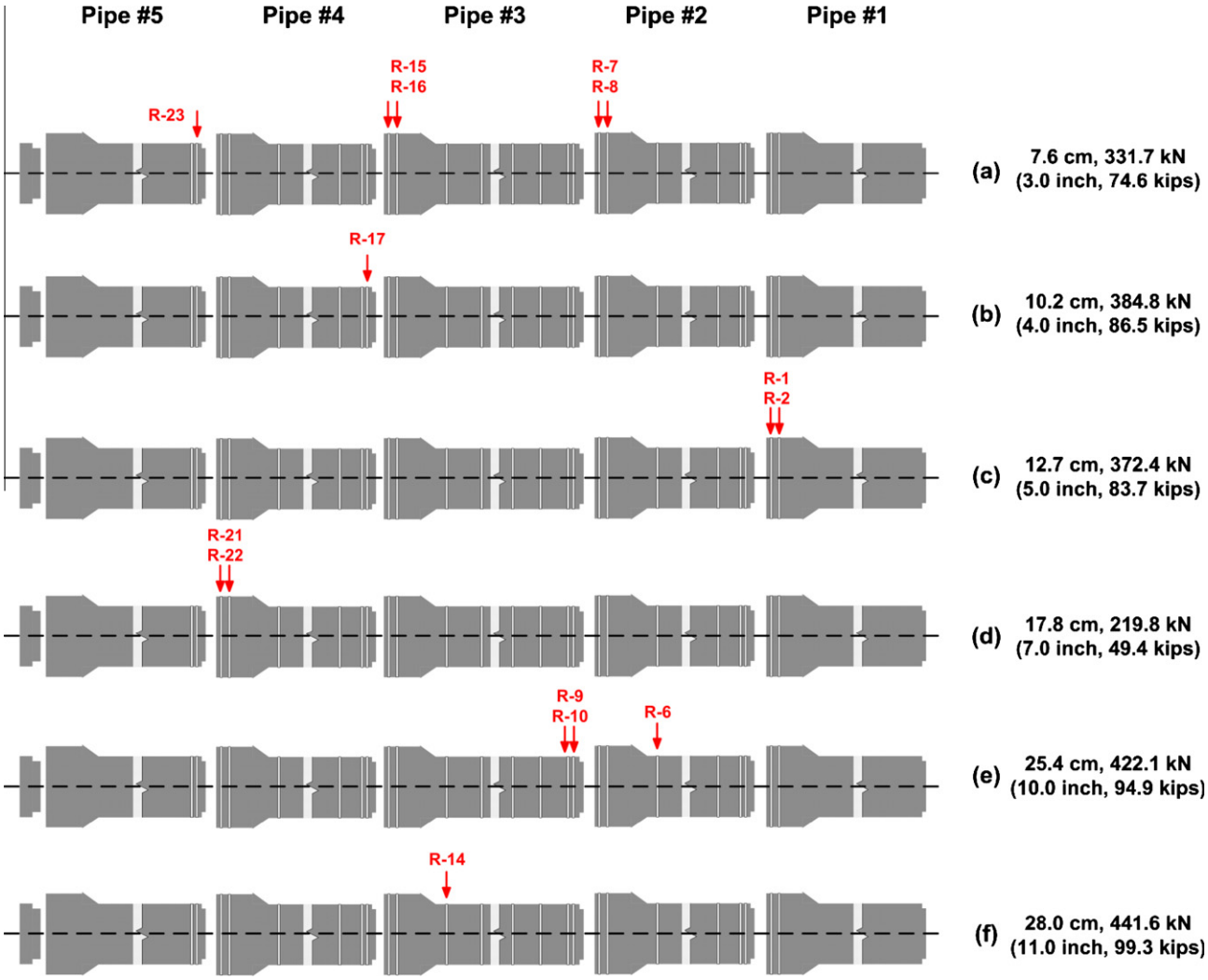

Fig. 8. Location of the detected damage by sensors. Arrows indicate the location of the damage captured by conductive surface tape (CST) sensors.

which might be due to the visco-elastic behavior of the soil. The visco-elastic behavior of soil can be seen in Fig. 6a especially during the relaxation period after the fourth and fifth displacement steps where the actuator load decreases while the displacement is constant. During the relaxation period after the fifth displacement step, a relative movement of the joint is detected at Joint 3 by the magnetic sensors (Fig. 11c). During the seventh displacement step, the magnetic sensor at Joint 1 detected damage, which is most likely associated with telescoping effects due to high compressive forces. Further damage using magnetic sensors is captured after the tenth displacement step.

7.4. Acoustic emission

Fig. 12 shows the average captured acoustic energy per sensor at Joints 2, 3, and 4. The amount of energy captured at Joints 2 and 3 are orders of magnitude larger than the amount of energy captured at Joint 4. This is consistent with the results from the CST and magnetic sensors in that the damage to Joints 2 and 3 was greater than at Joint 4. A significant amount of energy is captured during the first two displacement steps. This is consistent with the results shown in Fig. 7 where the damage was observed at Joints 2 and 3. Note that in all cases acoustic activity starts before any damage is detected by CST sensors in Fig. 7. A sudden increase of acoustic energy at Joint 4 was observed after the seventh displacement step. This observation is consistent with the signals received from CST and magnetic sensors. Also a significant decrease in load was observed at this actuation step (Fig. 6b).

A significant increase in acoustic energy is observed during the eighth displacement step at all joints. However, no signals from CST and magnetic sensors are received during this step (see Fig. 7) because the majority of the sensors installed at Joints 2 and 3 failed previously. During the relaxation period after the tenth displacement step no acoustic activity is captured; however, during this period signals from CST and magnetic sensors indicate damage at Joint 2 and Pipe Segment 2. This suggests that the damage to the joint occurred during the displacement and that the delay in the CST sensors might be due to the widening of the crack and the commensurate rupture of the CST.

Fig. 13 shows the cumulative acoustic energy at each joint categorized in three groups based on peak amplitude of the acoustic signal: <60 dB, 60 to 80 dB, and >80 dB. Smaller amplitudes can generally be attributed to the movement of the soil, micro-cracking of the concrete pipe, or cracking of the concrete far away from the sensor. High amplitude acoustic activity is generally associated with discrete cracking in the close vicinity of the sensor. Fig. 13 shows that the cumulative acoustic energy from high amplitude waves increases significantly after the eighth displacement step.

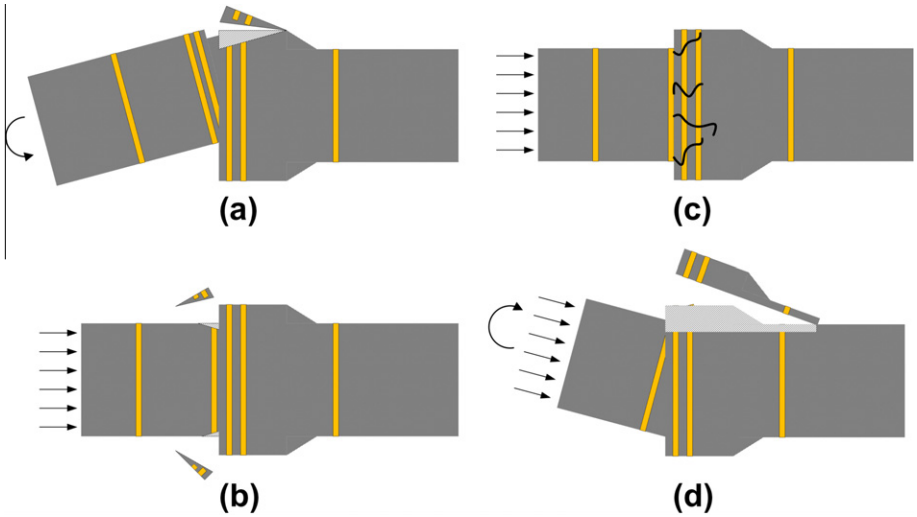

Fig. 9. Schematic illustration of (a) failure of bell due to angular rotation, (b) wedge-breaking due to compressive force, (c) failure due to telescoping and (d) failure of the joint due to rotation and telescoping.

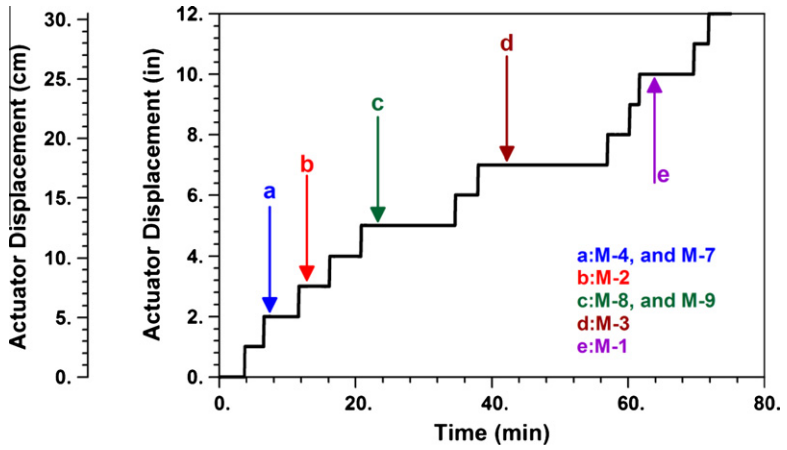

Fig. 10. Sequence of signals received from magnetic (M) sensors in relation to the actuator displacement.

This indicates extensive damage to the joints. The cracking at Joints 2 and 3 continues up to the tenth displacement step (i.e., 10-in. displacement).

7.5. Conductive grout

Fig. 14 illustrates the results of resistance measurements of the conductive grout at Joint 4. The resistance results are normalized to the maximum value measured. The normalized value of the resistance can be considered as an indirect measure of damage. As may be observed in Fig. 14, the resistance of the grout increases even at early stages of loading and continues to increase up to end of the seventh displacement step and then reaches the maximum value corresponding to the complete damage at the joint. This is consistent with the reduction of the loads (actuator and axial) in the seventh displacement step in Fig. 6b.

All three sections of Joint 4 approximately follow the same trend of resistance increasing; this indicates that the damage is almost uniformly distributed around the joint (i.e., telescoping). The majority of the damage is accumulated in the joint up to the end of the third displacement step. These results are consistent with the results obtained from CST sensors in Fig. 7a (Fig. 8a) where the damage is detected at spigot section of the Joint 4.

7.6. Damage evolution

Generally, the results provided above clearly show that the damage detected by the different sensor types is consistent. AE detected the damage before it was captured by CST and magnetic sensors (Fig. 12). The resistance increase of conductive grout due to telescoping damage (Fig. 14) is consistent with the decrease of axial and actuator loads (Fig. 6b). In combination, the sensors provide information on the types and order of damage that can occur in segmental concrete pipelines.

During the first four displacement steps (Figs. 8a and b, and 11a and b), the majority of the damage to the pipeline was concentrated close to the fault line. This is supported by the measurements taken by the CST, magnetic, and acoustic emission sensors. With an increase in displacement, particularly during the fifth and seventh displacement steps (Figs. 8c and d, and 11c and d), the damage had spread along a larger length of the pipeline. This can be seen in Fig. 7, and is confirmed by the decrease in the axial loads and actuator load (Fig. 6b).

Further damage to the pipeline is captured during the eighth displacement step by AE (Fig. 12). After the tenth and eleventh displacement steps, the damage propagates away from the joints and caused longitudinal cracks along of the Pipe Segments 2 and 3. The

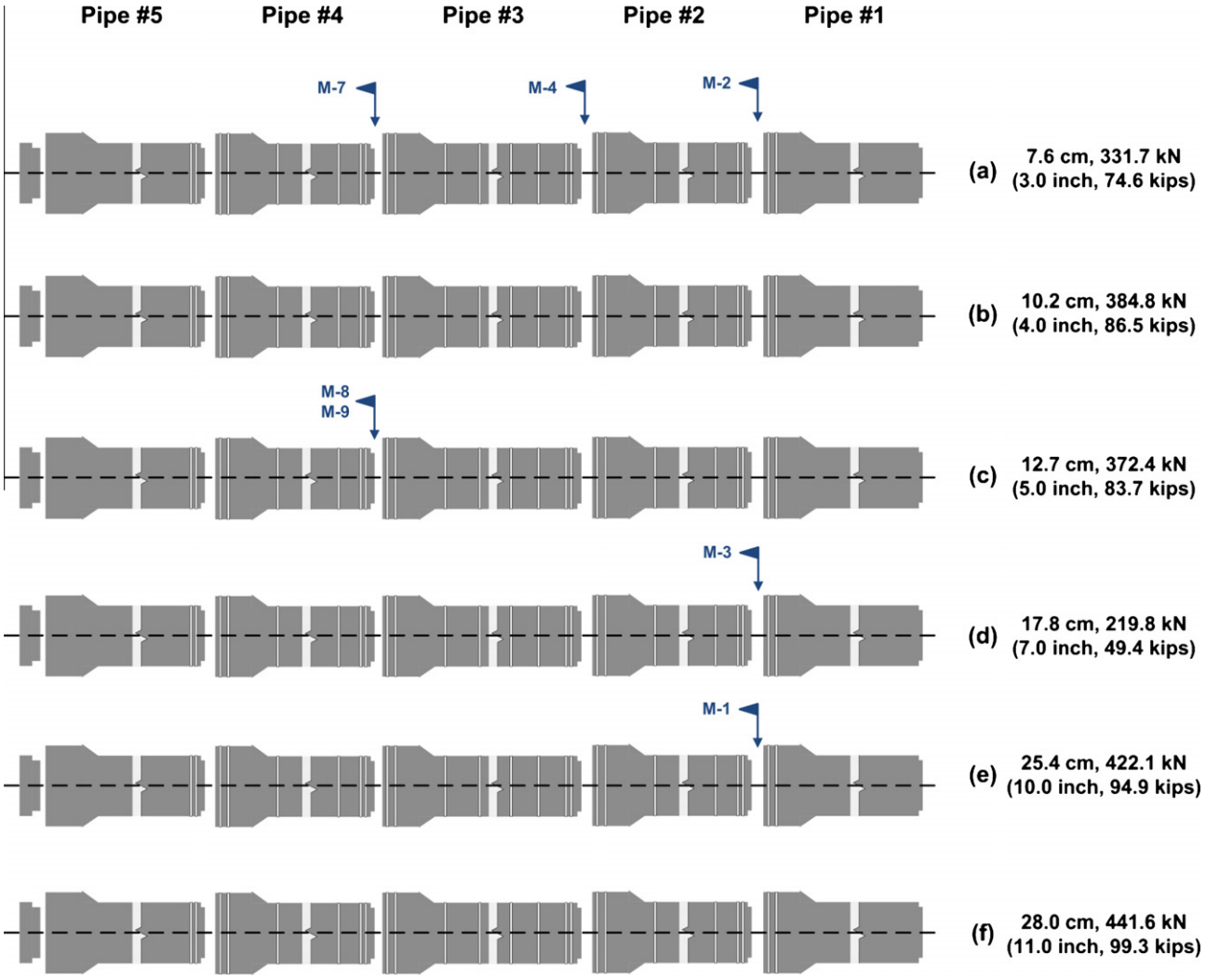

Fig. 11. Location of the detected damage by sensors. Flags indicate the location of the damage captured by magnetic (M) sensors.

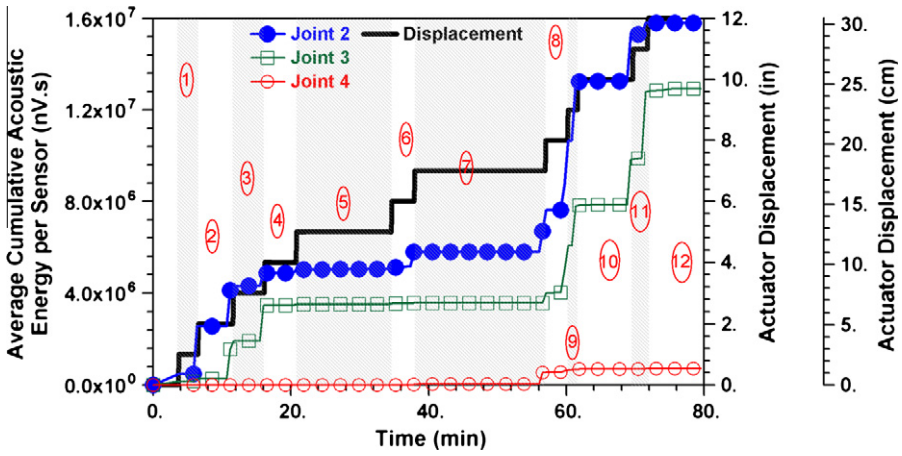

Fig. 12. Average captured cumulative acoustic energy.

sensors installed 30 cm (≈1 ft) away from the end of the bell section detected this damage (Figs. 8e and f and 11e and f).

In summary, the damage evolution in the segmented concrete pipeline can be considered in three stages. In the first stage (Figs. 8a and b, 11a and b), the majority of the damage is localized at the joints in the vicinity of the fault line. This stage can be thought of as a plastic hinge formation. Slight damage to the joints away from the fault line can be expected in this stage due to compressive forces along the pipeline and the "tightening" of the joints. In the second stage (Figs. 8c and d, 11c and d), the damage in the

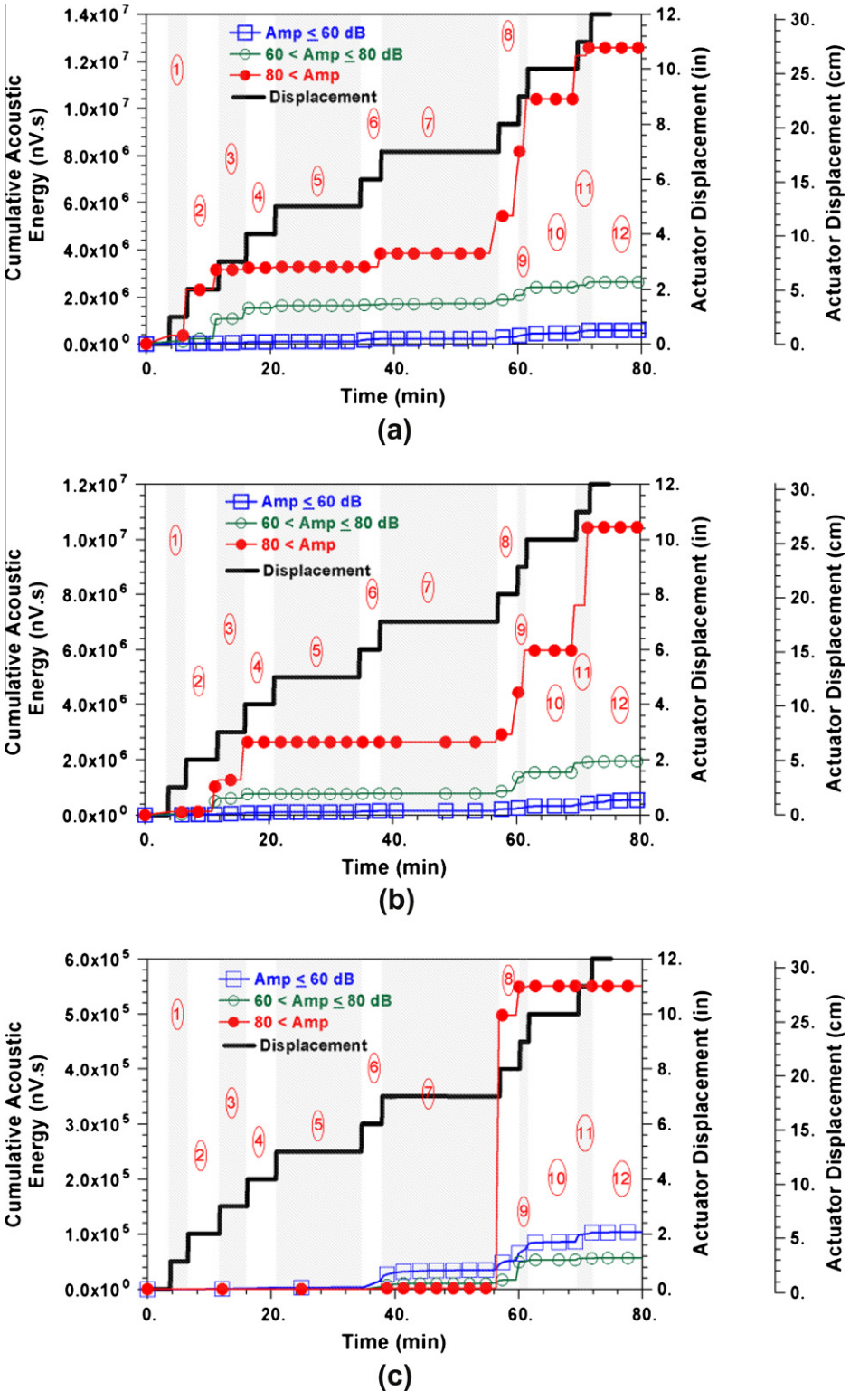

Fig. 13. Average captured cumulative acoustic energy at Joints (a) 2, (b) 3, and (c) 4.

pipeline spread along larger sections of the pipeline, and the rate of damage decreases at the joints in the immediate vicinity of the fault line. This stage can be thought of as damage distribution. In the third stage (Figs. 8e and f, 11e and f), the damage spreads to the body of the pipe segments in the vicinity of the fault line. The damage at this stage becomes severe and results in large longitudinal cracks. This stage is effectively a pipe rupture stage.

7.7. Visual observations after excavation

At the end of the experiment the pipeline was excavated and visually inspected. Fig. 15a through 15d illustrate the damage that developed during the test at Joints 1–4. Clearly, each of these joints was damaged. The observed damage is in agreement with the damage detected using the sensing methods. Specifically, the CST

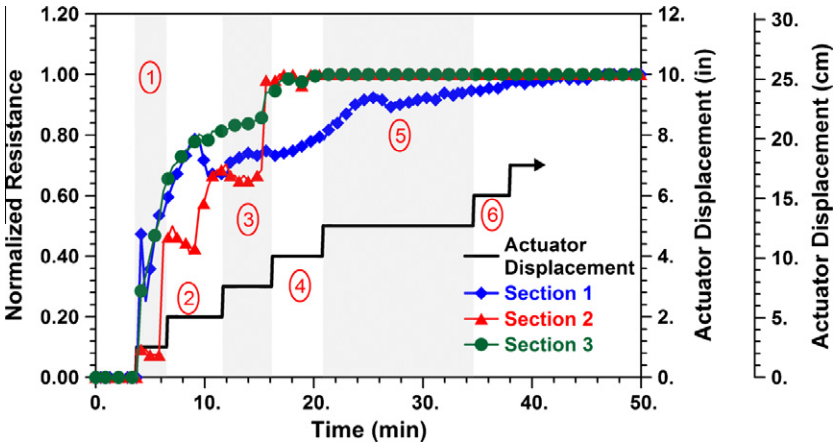

Fig. 14. Resistance increase of conductive grout due to damage at Joint 4.

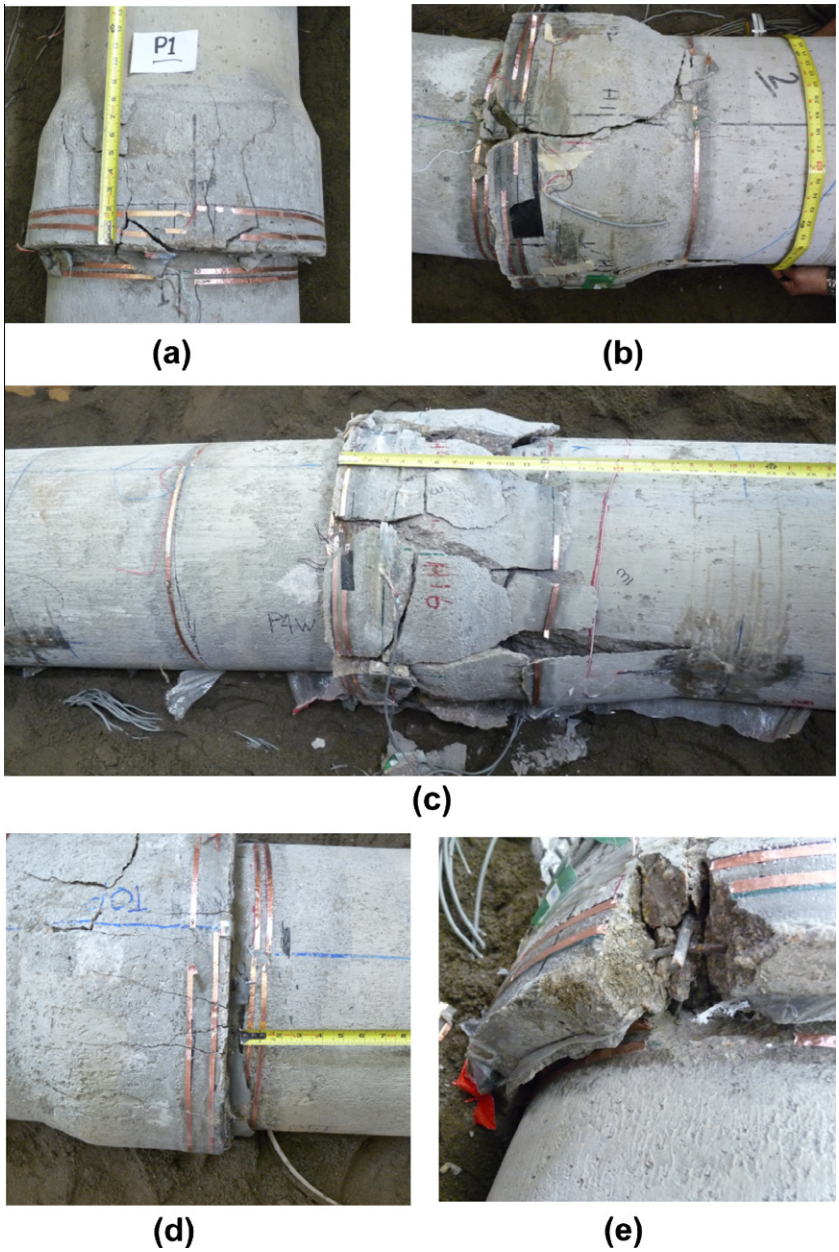

Fig. 15. Damage to joints observed after excavation (a) Joint 1, (b) Joint 2, (c) Joint 3, (d) Joint 4, and wedge-breaking type of damage seen in Joint 2.

sensors installed on the bell section of the joints detected damage at multiple points. The damage detected using CST and magnetic sensors is shown in Fig. 8 and Fig. 11 respectively. Extensive damage was observed at the bell sections of all four joints. Figs. 15b and c illustrate the damage to Joints 2 and 3, which were the most severely damaged. Large longitudinal cracks propagating away from the bell section can be seen. This damage was captured by CST sensors as shown in Figs. 8e and f.

The types of damage illustrated in Fig. 9 can be seen in the photographs shown in Fig. 15. Figs. 15b and c show the damage to Joints 2 and 3, which appear to have rotated and telescoped (Fig. 9d). It should be remembered that the photographs in Fig. 15 show damage at the time of excavation, however, the damage to Joints 2 and 3 increased progressively over time, from wedge-breaking damage to the spigot (Fig. 9b) to telescoping and crushing of the bell (Fig. 9c), and eventually to rotational and telescoping type failure (Fig. 9d). The wedge-breaking type of damage that was observed at Joint 3 is shown in Fig. 15e. The damage to Joints 1 and 4 is similar to the schematic illustration shown in Fig. 9c.

Except for the damage to Pipe Segments 2 and 3 that was detected by the CST sensors R-6 and R-14 (Figs. 8e and f), no other visually observed damage was found on the pipe segments away from the joints (along the pipe length).

8. Conclusions

This paper presented results from an experimental study that used a variety of sensing methods to assess damage development in a buried segmental concrete pipeline subjected to a concentrated transverse permanent ground displacement (PGD). The sensing methods included conductive surface tape, conductive grout, magnetic sensors, and acoustic emission. In addition, load displacement measurements were used to monitor the damage development. These methods enabled tracing of the damage propagation in the pipeline.

The sensing approaches captured the damage development in the segmental concrete pipeline, and the damage was consistent with the visual inspection after excavation of the pipeline.

The sensing methods used provided the time- and location-dependent information on damage development in the pipeline. Two types of damage were primarily observed: failure of joint due to relative rotation of bell-and-spigot and telescoping and crushing of the joints.

The results indicated that the majority of the damage in segmental concrete pipelines occurred at the bell sections of the joints in the pipeline. Damage was also observed away from the joints in the pipe segments in the immediate vicinity of the fault line. Telescoping, caused by axial forces, introduced considerable damage to segmental concrete pipelines. While damage due to shear forces is more severe in the vicinity of the fault line, damage due to telescoping affects a larger section of the pipeline.

Three stages of damage were observed. In the first stage, the majority of the damage occurred at the joints in the immediate vicinity of the fault line. This began with as little as 5.1 cm (2 in.) displacement along the fault line. The damage in the second stage began to occur after 12.7 cm (5 in.) displacement along the fault line. The damage in the second stage was more distributed along the pipeline and the rate of damage decreased at the joints in the immediate vicinity of the fault line. This stage was accompanied by telescoping process. The third stage of the damage development started approximately after 25.4 cm (10 in.) of displacement along the fault line. In this stage the damage spread to the body of the pipe segments in the immediate vicinity of the fault line. The damage at this stage became severe and resulted in large longitudinal cracks in the body of the pipe segments. This stage is effectively a pipe rupture stage.

This paper presented results from a second iteration of testing a segmental concrete pipeline as a part of a four-year program. The main objectives of the work described in this paper were to (1) use sensing methods for damage detection of segmental concrete pipelines, and (2) provide insight to the damage evolution of segmental concrete pipelines in the vicinity of concentrated transverse permanent ground displacement.

The sensing methods implemented in the tests described in this paper will be used to optimize the methods to be used in the next two years of pipeline testing, and to design new sensing methods that are more economical for field applications.

Acknowledgments

This work was supported by the National Science Foundation under the NEES Program, Grant CMMI-0724022, and this support is gratefully acknowledged. Any opinions, findings, and conclusions or recommendations expressed in this material are those of the authors and do not necessarily reflect the views of the National Science Foundation. The large-scale testing was performed at the Large-Scale Pipelines Testing Facility at Cornell University that is a node in the George E. Brown, Jr. Network for Earthquake Engineering Simulation (NEES). The authors thank the Cornell staff for their outstanding help with the experimental program. In particular, the help of Mr. Tim Bond and Mr. Joe Chipalowsky is greatly appreciated. This work, in part, was conducted in the Pankow Materials Laboratory and the Materials Sensing and Characterization Laboratory at Purdue University, and the Laboratory for Intelligent Structural Technology at the University of Michigan.

References

[1] Services TAMC. Chile earthquake and tsunami update. Hawaii: Tripler Army Medical Center. Center for Excellence in Disaster Management and Humanitarian Assistance; 2010.
[2] Kim J, Lynch JP, Michalowski RL, Green RA, Pour-Ghaz M, Weiss WJ, et al. Experimental study on the behavior of segmented buried concrete pipelines subject to ground movements. In: Felix WH, Diaz AA, Shull PJ, Vogel DW, editors. Nondestructive characterization for composite materials, Aerospace engineering, civil infrastructure, and homeland security 2009. SPIE; 2009. p. 729419–10.
[3] Shinozuka M, Rose A, Eguchi R. Engineering and socioeconomic impacts of earthquakes. Buffalo, NY: Multidisciplinary Center for Earthquake Engineering Research; 1998.
[4] Eguchi RT. Mitigating risks to infrastructure systems through natural hazard reduction and design. In: Choi C-K, Penzien J, editors. International Symposium on Public Infrastructure Systems Research. Seoul, Korea; 1995.
[5] Chang SE, Seligson HA, Eguchi RT. Estimation of the economic impact of multiple lifeline disruption: memphis light, gas and water case study. Buffalo, NY: Multidisciplinary Center for Earthquake Engineering Research; 1996.
[6] Chen W-F, Scawthorn C. Earthquake engineering handbook. New Directions in Civil Engineering. New York: CRC Press; 2002.
[7] Ballantyne D, Chung R, O'Rourke T, Schiff A. Performance of lifeline systems, the January 17. 1995 Hyogoken-Nanbu (Kobe) earthquake, performance of structures, lifelines and fire protection systems. Washington, DC: National Institute of Standards and Technology; 1996.
[8] Ballantyne D. Water system performance in the Great Hanshin (Kobe) earthquake. 1995 American Water Works Association Annual Conference. Anaheim, CA: American Water Works Association, Denver, CO; 1995.
[9] O'Rourke TD, Grigoriu MD, Khater MM. A state of the art review: seismic response of buried pipelines. In: Sundararajan C, editor. Decade of progress in pressure vessel technology. New York: American Society of Mechanical Engineers; 1985.
[10] Eguchi RT. Seismic vulnerability models for underground pipes. Earthquake behavior and safety of oil and gas storage facilities, buried pipelines and equipment, PVP-77. New York: American Society of Mechanical Engineers; 1983. p. 368–73.
[11] Porter KA, Scawthorn C, Honegger DG, O'Rourke TD, Blackburn F. Performance of water supply pipelines in liquefied soil. Fourth US–Japan Workshop on Earthquake Disaster Prevention for Lifeline Systems. Los Angeles, CA; 1991. p. 3–17.
[12] Heubach WF. Seismic damage estimation for buried pipeline systems. Fourth US conference on lifeline earthquake engineering. New York: American Society of Civil Engineers, Technical Council on Lifeline Earthquake Engineering; 1995. p. 312–9.

[13] Eidinger JM, Maison B, Lee D, Lau B. East Bay municipal utility district water distribution damage in 1989 Loma Prieta earthquake. Fourth US Conference on Lifeline Earthquake Engineering. American Society of Civil Engineers, Technical Council on Lifeline Earthquake Engineering; 1995. p. 240–7.
[14] Kim J, O'Connor S, Nadukuru S, Lynch JP, Michalowski R, Green RA, et al. Behavior of full-scale concrete segmented pipelines under permanent ground displacements. In: Kundu T, editor. Health Monitoring of Structural and Biological systems 2010. SPIE; 2010. p. 76500U-U-11.
[15] Bradshaw AS, daSilva G, McCue MT, Kim J, Nadukuru SS, Lynch J, et al. Damage detection and health monitoring of buried concrete pipelines. In: Oka FMAKS, editor. International Symposium on Prediction and Simulation Methods for Geohazard Mitigation. Kyoto, Japan; 2009. p. 473–8.
[16] O'Rourke TD, Gowdy TE, Stewart HE, Pease JW. Lifeline performance and ground deformation in the Marina during 1989 Loma Prieta Earthquake. Third Japan–US Workshop on Earthquake Resistant Design of Lifeline Facilities and Countermeasures for Soil Liquefaction. San Francisco; 1991. p. 129–46.
[17] Krathy RG, Salvadori MG. Strength and dynamic characteristics of gasket-jointed concrete water pipelines. New York: Weidlinger Associates; 1978.
[18] Ayala G, O'Rourke M. Effects of the 1985 Michoacan earthquake on water systems and other buried lifelines in Mexico. Buffalo, NY: Multidisciplinary Center for Earthquake Engineering Research; 1989.
[19] Sun S, Shien S. Analysis of seismic damage to buried pipelines in Tangshan earthquake. Earthquake behavior and safety of oil and gas storage facilities, buried pipelines and equipment, PVP-77. New York: American Society of Mechanical Engineers; 1983. p. 365–7.
[20] Prior JC. Investigation of bell and spigot joints in cast iron water pipes. Ohio State University; 1935.
[21] El Hmadi K, O'Rourke MJ. Seismic wave effects on straight jointed buried pipeline. Buffalo, NY: Multidisciplinary Center for Earthquake Engineering Research; 1989.
[22] Palmer MC, O'Rourke TD, Stewart HE, O'Rourke MJ, Symans M. Large displacement soil-structure interaction test facility for lifelines. Eighth US National Conference on Earthquake Engineering, San Francisco, CA2006.
[23] O'Rourke TD, Bonneau A. Lifeline performance under extreme loading during earthquakes. In: Pitilakis KD, editor. Earthquake Geotechnical Engineering. Dordrecht, Netherlands: Springer; 2007. p. 407–32.
[24] ASTMC76. Standard specification for reinforced concrete culvert, storm drain, and sewer pipe. West Conshohocken, PA: ASTM International; 2010.
[25] ASTMC655. Standard specification for reinforced concrete d-load culvert, storm drain, and sewer pipe. West Conshohocken, PA: ASTM International; 2009.
[26] AWWAC300. Standard for reinforced concrete pressure pipe, steel cylinder type, for water and other liquids. Denver, CO: American Water Works Association; 2004.
[27] ASTMD2922. Standard test methods for density of soil and soil-aggregate in place by nuclear methods (shallow depth). West Conshohocken, PA: ASTM International; 2005.
[28] ASTMD2216. Standard test methods for laboratory determination of water (moisture) content of soil and rock by mass. West Conshohocken, PA: ASTM International; 2010.
[29] Pour-Ghaz M, Weiss J. Detecting the time and location of cracks using electrically conductive surfaces. Cem Conc Compos 2011;33:116–23.
[30] Raoufi K, Pour-Ghaz M, Poursaee A, Weiss J. Restrained shrinkage cracking in concrete elements: the role of substrate bond on crack development. ASCE J Civ Eng Mater; 2011. doi:10.1061/(ASCE)MT.1943-5533.0000247.
[31] Pour-Ghaz M, Poursaee A, Spragg R, Weiss J. Experimental methods to detect and quantify damage in restrained ring test. West Lafayette. School of Civil Engineering, Purdue University; 2010.
[32] Poursaee A, Weiss WJ. An automated electrical monitoring system (AEMS) to assess property development in concrete. Automat Constr 2010;19(4):485–90.
[33] Scott IG. Basic acoustic emission. New York: Gordon and Breach Science; 1991.
[34] Yuyama S, Ohtsu M. Acoustic emission evaluation in concrete. Acoust Emission – Beyond Millennium 2000:187–213.
[35] Puri S, Weiss J. Assessment of localized damage in concrete under compression using acoustic emission. ASCE J Civ Eng Mater 2003;18(3):325–33.
[36] Puri S. Assessing the development of localized damage in concrete under compressive loading using acoustic emission. West Lafayette, Purdue University; 2003.
[37] Ouyang CS, Landis E, Shah SP. Damage assessment in concrete using quantitative acoustic-emission. J Eng Mech – ASCE 1991;117(11):2681–98.
[38] Ohtsu M, Shigeishi M, Sakata Y. Nondestructive evaluation of defects in concrete by quantitative acoustic emission and ultrasonics. Ultrasonics 1998;36(1–5):187–95.
[39] Ohtsu M, Shigeishi M, Iwase H, Koyanagi W. Determination of crack location, type and orientation in concrete structures by acoustic-emission. Mag Concr Res 1991;43(155):127–34.
[40] Landis EN, Baillon L. Experiments to relate acoustic emission energy to fracture energy of concrete. J Eng Mech – ASCE 2002;128(6):698–702.
[41] Kim B, Weiss J. Using acoustic emission to quantify damage in restrained fiber reinforced cement mortars. Cem Concr Res 2003;33(2):207–14.
[42] Pour-Ghaz M, Weiss J. Quantifying damage due to aggregate expansion in cement matrix. In: Ideker JH, Radlinska A, editors. Advances in the Material Science of concrete. American Concrete Institution; 2010.
[43] Garboczi EJ, Snyder KA, Douglas JF, Thorpe MF. Geometrical percolation-threshold of overlapping ellipsoids. Phys Rev E 1995;52(1):819–28.